LMR STEAM GENERATOR BLOWDOWN WITH RETRAN

T. Y. C. Wei
Reactor Analysis and Safety Division
Argonne National Laboratory

CONF-8511130--1

DE86 004069

INTRODUCTION AND CONCLUSIONS

Currently, there is an ongoing effort to draw from the experiences of the nuclear industry for the past twenty years to develop innovative reactor concepts which would answer the concerns that have been brought up in the operating, licensing and construction environment of the recent past. As part of this development effort ANL has proposed the IFR (Integral Fast Reactor) concept,[1] key features of which are metal fuel, a pool-type reactor design, and integral reprocessing. The IFR concept is currently being applied to small reactors which would be built in multiple power paks together with an integrated fuel cycle facility. The IFR concept provides inherent safety characteristics and proliferation resistance. The development has proceeded to where system transient analyses have been performed to determine the adequacy of the response of the plant protection system (PPS), the performance of certain inherent safety features and the margin to plant damage limits. One of the transients which is being considered in the "FSAR Chapter 15" analyses of anticipated LMR (Liquid Metal Reactor) transients is the fast blowdown of a steam generator upon inadvertent actuation of the liquid metal/water reaction mitigation system. In the unlikely event of a steam generator tube leak, the mitigation system is designed to evacuate the steam generator before significant pressure and hydrogen buildup result from the sodium water reaction. In the case of blowdown of only the water side, it is important to assure that thermal stress limits have not been violated, since with the sodium side intact a hot shock from the steam generator can quickly propagate through the IHTS (Intermediate Heat Transport System) pump and ultimately the IHX. To perform such a steam generator blowdown analysis a stand-alone steam generator model for the IFR plant was constructed using RETRAN. The isolation of the steam generator from the remainder of the system is possible for the period of the blowdown because the results show that the blowdown is over in a matter of about a second. This time interval is significantly smaller than the loop cycle time in the intermediate heat transport system. Perturbations in the steam

generator sodium inlet at normal flow conditions. In addition, the results show that the feedwater line break characteristics of the transient dominate over the steam line break characteristics. The steam line dump induced cooldown is of limited duration and magnitude. The steam generator thermal response is essentially that induced by an adiabatic boundary condition established at the water side of the tube metal. The thermal transient should be of little consequence to the steam generator tubes as the tube time constant is small. Thicker structures such as nozzles await further evaluation through thermal stress analyses.

IFR SYSTEM DESIGN

The IFR concept is being applied in a small sodium cooled, pool type, metal fueled reactor to be built in multiple power paks in conjunction with an integrated fuel cycle facility. The IFR concept is to be demonstrated in the EBR-II facility. Figure 1 is a schematic of the overall EBR-II facility. EBR-II is a sodium cooled fast breeder reactor[2] generating 20 MWe located at ANL-West in Idaho Falls. The plant and its associated fuel cycle facility were built approximately 20 years ago. It is a pool type plant, with the reactor, primary coolant pumps and intermediate heat exchanger (IHX) immersed in a large volume of sodium in the primary pool. The IFR fuel cycle facility will be based on modifications of the facility built and operated for the EBR-II plant. A large amount of work has already been carried out on the development of advanced pyrometallurgical techniques for reprocessing and fuel cycle economics trade off studies are underway. The use of metal fuel leads to a compact reprocessing process which is diversion resistant and does not require large scale deployment for competitive economics. LWR reprocessing is not a prerequisite for the startup fissile. Furthermore, metal fuel leads to improved inherent safety advantages in conjunction with the pool concept.

Figure 2 shows a proposed reactor vessel configuration[3] for an IFR reactor while Figure 3 shows a simplified plant layout. The reactor core, the primary coolant pumps and the IHXs are immersed in a large volume of sodium in the primary pool. The reactor vessel contains basically the entire inventory of the primary sodium coolant and containment is its only function. Support of the internals is provided by the hanging core support structure which together with the vessel is suspended at the top flange from the same conical skirt. The deck is supported by the same skirt. There is a backup support system denoted as RIBSS (Reactor Internals Backup Support System). The vertical redan which divides the primary pool into hot outlet pool and cold inlet pool is also supported by the core support structure. Cold sodium from the cold pool is pumped by the centrifugal primary pumps into the inlet

Figure 1. EBR-II Reactor and Fuel Cycle Facility

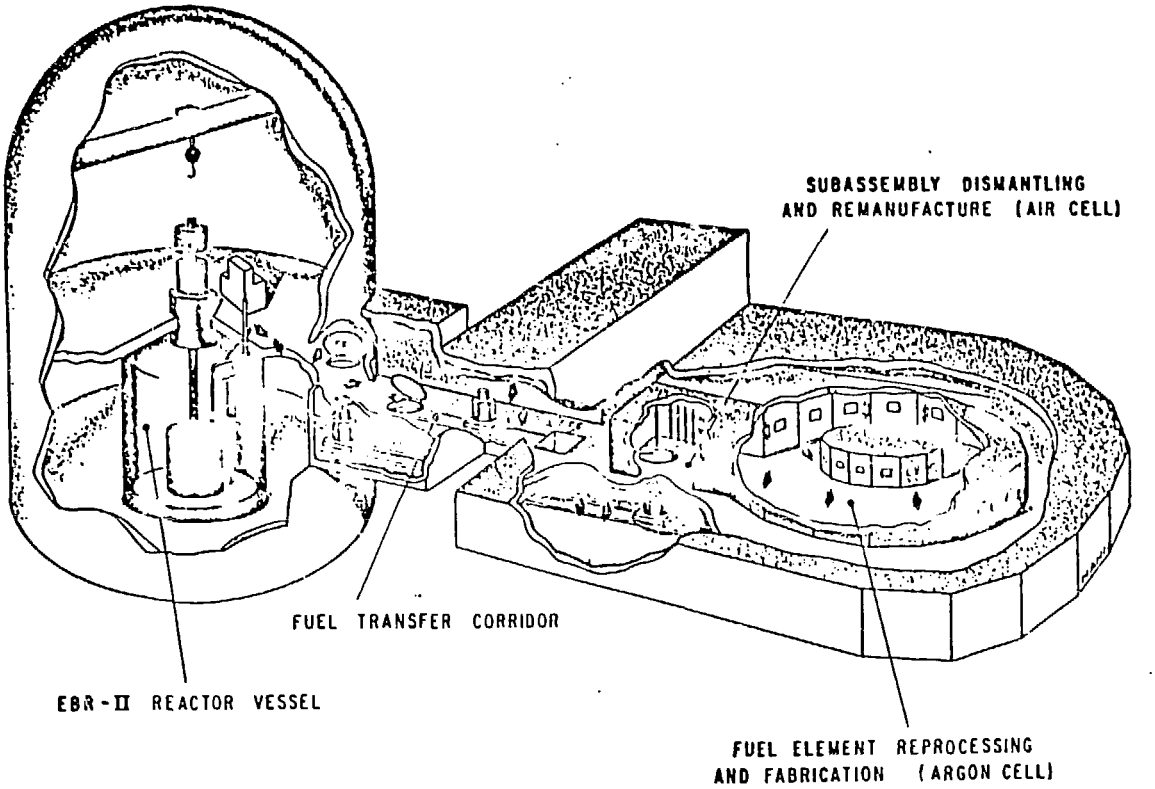

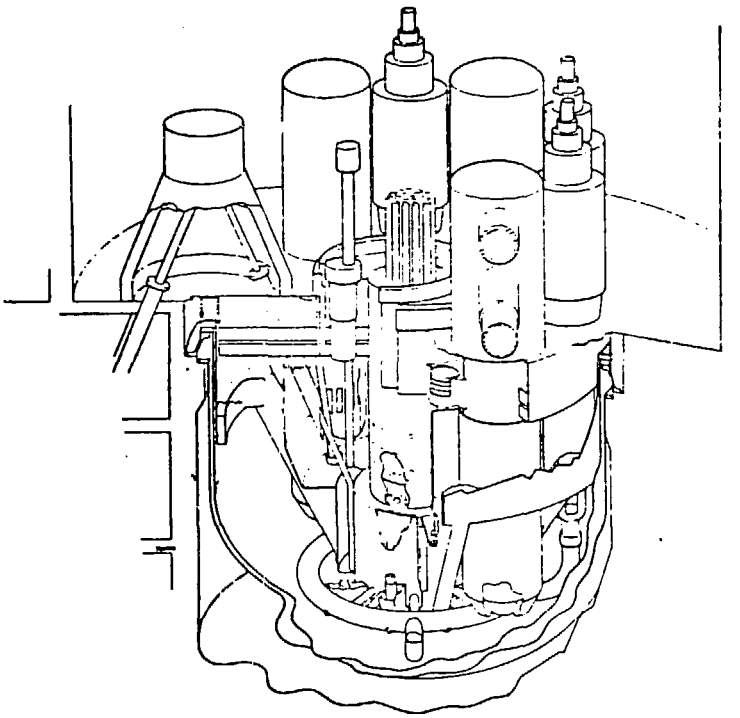

Figure 2. Reactor Assembly - Pictorial

Figure 3. One-Loop Plant Model

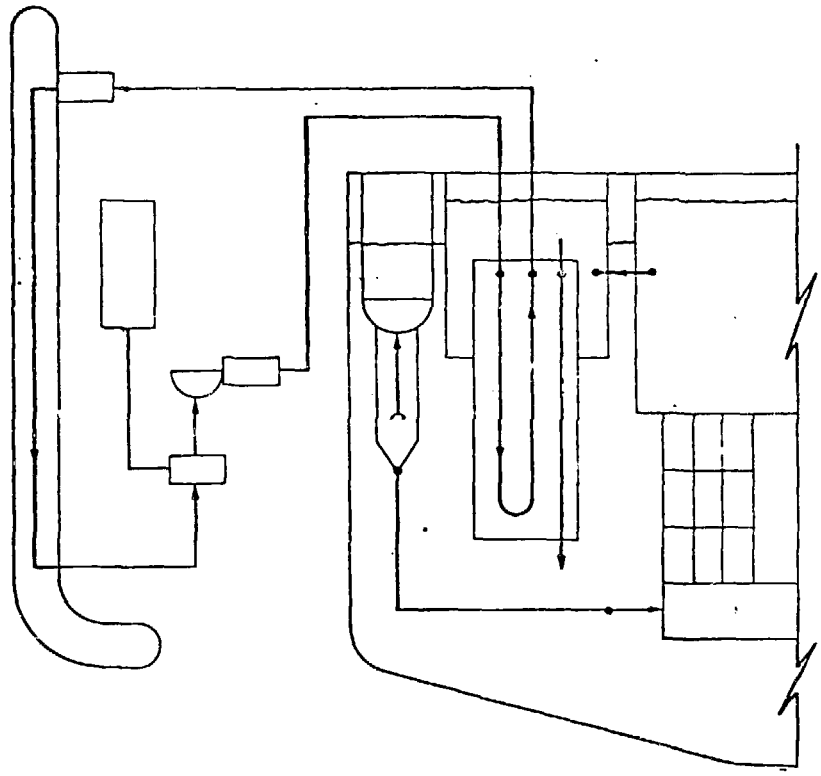

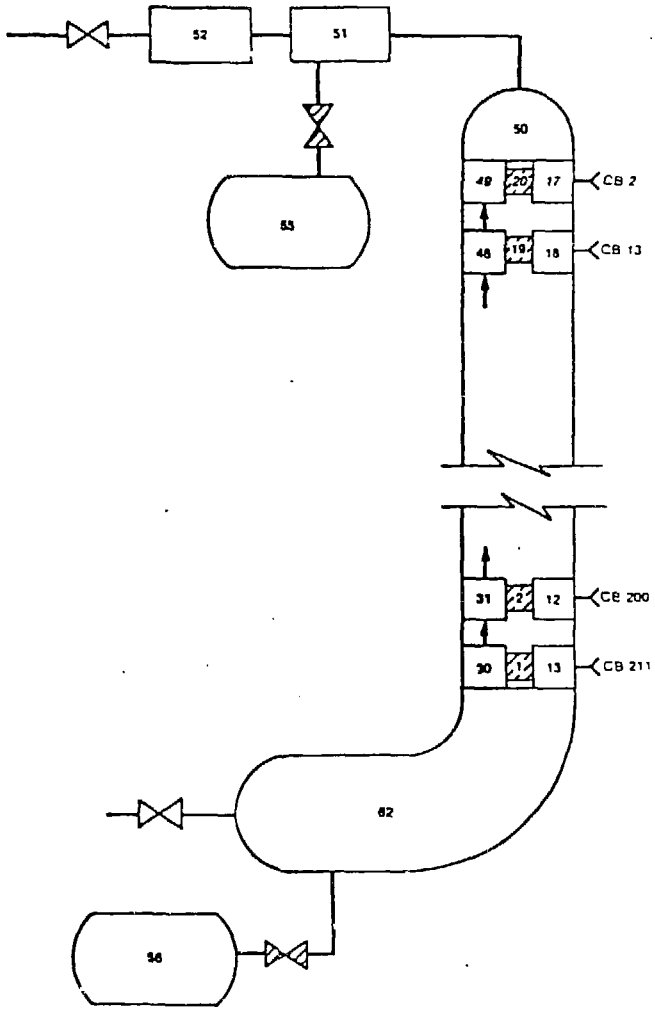

Figure 4. RETRAN Stand-alone Steam Generator Model

plenum and thence through the core and into the hot outlet pool. Elevation differences feeds the hot sodium into the inlet of the IHXs, past the tube bundle and into the cold pool. The only primary piping used is from the discharge side of the inlet pump to the core inlet plenum. The Intermediate Heat Transport System (IHTS) is a pipe system transporting sodium between the IHXs and the steam generators. There is one IHTS pump per IHTS loop and one steam generator per loop. The steam generator is a once through steam generator (OTSG) just as the B&W (Babcock and Wilcox) superheated steam generator is a once through generator. However, unlike the B&W OTSG the tube/shell combination has boiling in the tube side. The intermediate sodium flow is in a counter current flow arrangement on the shell side.

A comparison of "typical" design values will be presented next in order to provide a quantitative measure. It should be remembered that the values presented are only approximately representative and therefore should not be extrapolated further as further extrapolation may lead to inconsistent conclusions.

There are some significant geometrical differences between the IFR and the PWR. There is a considerable difference in the primary side volumes and inventory. The IFR has a significantly larger thermal inertia. The cover gas volume is also a factor larger than the pressurizer volume of the PWR and the sodium volume coefficient of expansion is smaller. Pressure transients caused by thermal cycling will be better damped. The heights and therefore gravity elevation heads of the two systems are roughly comparable. The flow area in the two cores are comparable while the steam flow area in the IFR SG is also considerably smaller. The IFR steam generator inventory is also considerably smaller. Blowdowns and cooldowns will be of shorter duration and possibly have milder consequences.

Table I gives thermal hydraulics design data. The IFR primary and intermediate sides are basically at atmospheric pressures as compared to the significantly higher RCS pressure of the LWR. Chemical reactions asides, LOCA transients of the two systems would be expected to have considerably different temporal characteristics. The steam generator pressure of the IFR OTSG (once through steam generator) with its large superheat is, however, a factor of two larger than the LWR U-tube steam generator with its wet steam. This coupled with the smaller inventory should lead to much faster blowdowns. In general, the IFR coolant temperatures are higher thus leading to the higher efficiencies but the fuel temperatures are comparable even though the average linear power rating is higher. This is due to the higher thermal conductivity of the IFR and it translates to comparable specific stored energy in

the fuel as the specific heats of the two fuel types are close. This factors in the lower peaking factors of the IFR.

The pressure drops on the primary side are comparable for the two systems but the pressure drop in the steam generator is significantly higher for the IFR. The lower steam flow rate is not compensated for by the drastic reduction in the flow area. The mass flux rate is noticeably higher and this combined with the considerably smaller hydraulic diameter requires a higher pressure drop. The high mass flux rate is required to obtain the necessary heat transfer rate in the superheat region which for the IFR is a considerable portion of the heat transfer region. The steam generator heat fluxes are significantly higher for the IFR while the core heat fluxes are similar.

Combining the geometry information and the design thermal hydraulics information gives certain plant characteristics which are important for transient analysis. It can be concluded that the adiabatic primary system heatup rate is factors higher for the PWR. This is mitigated by the fact that the steam generator inventory can serve as a heat sink. The adiabatic heating rate for the fuel pin is lower for the PWR because of the lower power density and the smaller difference between the specific heats of the two fuel systems. The loop cycle times show that there is much less coupling between the primary and secondary side for the IFR. The small transport time couples the PWR primary and secondary sides quite tightly. For fast transients the short thermal time constant of the IFR metal pin implies that the coolant heat flux will follow the power much more closely than in the case of the larger PWR oxide pin. In addition, the lower reactivity feed back coefficients of the IFR could mean slower power turnaround for the more rapid transients. The difference in degree of subcooling implies a higher margin to boiling for the IFR. Finally, the respective volume coefficients of expansion show an order of magnitude higher value for the PWR. This coupled with the smaller pressurizer volume means that pressurization transients induced by thermal changes will be more severe for the PWR.

Table 1

Core Inlet Temperature	650°F
Core Outlet Temperature	950°F
Primary Cover Gas Pressure	15 psia
IHX Intermediate Inlet Temperature	900°F
IHX Intermediate Outlet Temperature	600°F
Intermediate Cover Gas Pressure	15 psia
Steam Generator Feedwater Temperature	500°F
Steam Generator Steam Temperature	850°F
Steam Outlet Pressure	2000 psia

RETRAN MODEL

The simulation of the water side of the OTSG for the IFR is relatively simple to implement. Boiling in tubes forms a large part of the experimental data base for the heat transfer correlations used in RETRAN-02.[4] The operating pressure is in the range of the operating pressures of the primary side of PWRs and significantly below the critical point of water so the polynominal formulation used for the thermodynamic properties of water should be adequate. The high mass flux rate and pressure may be in an extrapolation range for the heat transfer but experiments are underway to verify the validity of the correlations used. The HEM and dynamic slip options are available for the depressurization. Modelling of the water side with RETRAN should be an adequate treatment. The prime difficulty is in formulating the sodium side.

In the temperature and pressure range of interest sodium is well treated as approximately incompressible for this particular application. The hydraulic aspects of the sodium flow through the steam generator can also be decoupled from the heat transfer part of the problem, as the pumps are not tripped. A simple energy balance equation for the sodium would thus be sufficient to treat the sodium side

$$\frac{d}{dt}(m_i h_i) - \dot{p}\, v_i = \theta_i + (\Sigma_j\, h_j\, w_{ij})_i \qquad (1)$$

where

m_i = node mass
h_i = node enthalpy
v_i = node volume
θ_i = heat deposited in node i
p = pressure
w_{ij} = mass flow from node j to node i

With incompressibility this becomes

$$\dot{\overline{T}}_i = \frac{\theta_i + c_p\,(T_{i-1} - T_i)w}{m_i} \qquad (2)$$

with

$\overline{T}_i$ = node average temperature
T_i = node exit temperature
c_p = coolant specific heat

where a differentiation is now made between the nodal average temperature $\bar{T}_i$ and the nodal interface temperatures T_i. A simple enthalpy transport is used to relate the two which then gives the particular mesh structure used more detail in terms of the temperature

$$\dot{T}_i + \frac{4\ w\ T_i}{m_i} = \frac{2\ \theta_i}{m_i\ c_p} + \frac{4\ w}{m_i} \bar{T}_i \tag{3}$$

and

$$\theta_i = A_i\ u_i\ (T_{metal\ i} - \bar{T}_i) \tag{4}$$

with

A_i = node heat transfer area
T_i = heat transfer coefficient
$T_{metal\ i}$ = metal slab interface temperature

Equations (2) and (3) can be "programmed" into the simulation by using the control blocks available. The Lag compensation, integrator and other blocks are quite capable of modelling these sodium side equations as the control system is a very flexible and powerful tool. As it was unclear what kind of numerical scheme would be ultimately required to couple these equations with the standard RETRAN thermal hydraulic models it was decided to use the valve area input variables as dummy storage locations for certain of the intermediate computed results as these variables are accessible to the control system blocks. Ultimately these were not utilized but this possibility demonstrates the flexibility of the control system blocks.

The connection between the water side and the sodium side is effected through the heat transfer rate θ_i. To model this connection the control system controlled non-conduction heat exchanger model and the nodalization of Fig. 4 was used. Heat at a rate determined by Eq. (4) is deposited through the system of control blocks 2-211 in volumes 17, 18, ... This heat is conducted through the chain of heat slabs 1-20, which simulate the steam generator tube walls, into the chain of water side volumes 30-49. These water side volumes are connected by junctions represented by arrows in the nodalization diagram and the combination represents the tube/shell region of the steam generator. Volumes 50 is the steam dome while while volumes 51 and 52 represent the steam line. Volume 62 is basically the feedwater inlet plenum

homogenized with the stagnant volume below the sodium outlet volume through which the steam tubes run. Volumes 55 and 56 are the dump volumes. The valves needed as dummy storage locations are implemented as part of the problem separate from the steam generator. As RETRAN will not accept multiple junctions between the same volumes a separate chain of large volumes was created at the same pressure so that there would be no time step limitations from this part of the simulation. The valves are located on the corresponding junctions.

Initially, volumes 17, 18, ... were treated as very small water volumes with large input heat transfer coefficients for the heat slab/volume interface heat transfer so that the resistance would be insignificant and the heat capacity negligible. However, this forced the RETRAN time step to be less than $\sim 10^{-6}$ seconds and led to what was probably a numerical instability problem. Round off is suspected but was not established as the cause. The volumes were then assumed to be an extension of the tube metal and the volumes and heat transfer coefficients were increased so that the time step could be increased to $\sim 10^{-3}$ seconds. This assumption can be made because the geometrical information, volume, areas and thicknesses can be input separately. In any case, fouling factors had to be ultimately used to obtain the design heat transfer rates and the extra metal volume only amounted to ~ 10% of the design tube heat capacity. Even with this change and a better estimate for the initial temperature distributions numerical problems were still encountered. Apparently the code makes a pass through the steady state initializer at t = 0 for the conduction equation as initial heat slab temperatures cannot be input. This causes a quick deterioration of the temperatures and pressures in the volumes 17, 18, ... Linking up the volumes with junctions and simulating the problem as an artificial BWR with the core located in the inlet plenum volume 62 did not resolve the numerical difficulty.

The RETRAN algorithm is most suited for a problem with primary and secondary sides. The standalone steam generator approach was therefore abandoned and a plant model was implemented by constructing an artificial primary loop linking volumes 17, 18, ... with the separate chain of volumes created for the valve storage variables. The nodalization diagram of Fig. 4 is still valid except that volumes 17, 18, ... are now connected by junctions and the inlet and outlet are connected to an artificial primary loop made of 20 volumes/junctions. Low flow, low power and small volumes are used in the dummy primary loop which runs on natural circulation as the core is located at an elevation lower than the steam generator. The steady state initializer cannot be used as the steam generator boiling is in the tubes and not on the shell

side. This is a minor inconvenience. The major difficulty of algorithm problems encountered with the standalone generator approach have disappeared with this reformulation in terms of a plant system. With a proper choice of initial temperature distributions the plant model converges to a steady state in ~ 10 seconds during a null transient. The correct heat balance is effected from the sodium side to the water side through the control blocks and the nonconduction heat exchanger. A temperature front propagation test through the sodium side indicated good spatial resolution on the sodium side.

Table 2 shows the valve times and set points used for the transient analyses. The blowdown valves are on both the steam dome and the feedwater inlet plenum leading to volumes 55 and 56. The isolation valves are on the steam line (junction to vol. 52 from boundary) and on the feedwater line (junction to volume 62 from boundary). Valve blowdown areas used the full steam/feed water line areas.

Table 2. Valve Data

MSIV closing time	0.5 secs
MFWIV closing time	0.5 secs
FW line blowdown valve opening time	0.5 secs
Steam line blowdown valve opening time	0.5 secs
Blowdown valve closing pressure	20 psia

TRANSIENT RESULTS

Prior to performing transient calculations a null transient was run to establish steady state as the steady state initializer could not be used. Some difficulties were encountered with meeting design conditions particularly in tube temperature drops and steaming rates which were overestimated for design geometrical information. This was attributed to the usage of fouling factors and uncertainty factors. It was therefore thought justifiable to adjust the sodium side heat transfer coefficient to achieve a reasonably close steaming rate as the water side coefficients are not adjustable through input. When experimental results are available this procedure will be reexamined. With this adjustment each null transient was run out to 10 seconds which is approximately the generator sodium transport time to obtain a quasi-steady state at which point closure of the isolation valves on both the steam and feed lines was initiated and simultaneously the steam/feed dump valves were opened. Depressurization continued until the set point of 20 psi was reached (basically atmospheric pressure) and closure of all the

dump valves was initiated. Initially the dynamic slip option was used to calculate the slip between the two phases as flashing occurred and the steam generator emptied. However, as the pressure gradient changed from being monotonic towards the steam outlet to a shape with a maximum towards the central region as flow exited from both ends of the generator, the dynamic slip option displayed numerical problems at the turning point. Negative pressures were obtained even with the reduction of the time step to 10^{-6} seconds. A switch to the HEM slip option resolved the negative pressure difficulties as the transition to a nonmonotonic pressure gradient became a smooth process with the depressurization to 20 psi proceeding without difficulty. As the void profiles at t = 0 are very close for the two slip options and as the emptying of the generator occurs in ~ 1 second, the choice of the HEM should not change the conclusions of this study significantly.

Figures 5 to 16 show results from the steam generator water side blowdown transient caused by the inadvertent actuation of the sodium/water reaction system on the water side only. The sodium side of the blowdown system is not actuated so the thermal shock of the water side blowdown will be propagated into the IHTS pump and ultimately the IHX. No pump trip is assumed. This coupled with the nonactuation of the IHTS sodium dump implies that IHTS pump and the IHX will see the hot shock in ~ few seconds.

Figure 5 which shows the pressure shows that the depressurization is over in ~ 1 second. The inventory of ~ few thousand lbs is insignificant compared to the ~ 10^5 lbs for a typical PWR. Figures 6 and 7 show the dump valve flow rates. Critical flow is initially reached in the feedwater line. Figures 8, 9, and 10 show the sodium side temperatures at three locations: the sodium inlet nozzle, an approximately midplane position and the sodium outlet nozzle. This transient has the characteristics of both a steam line break and a feedwater line break since inventory is dumped both through the top of the steam generator through the steam line and through the bottom of the generator through the feed water line. The sodium inlet nozzle location definitely shows a cooldown followed by a heatup. The cooldown is less pronounced at the midplane location while at the sodium outlet nozzle location at the bottom of the steam generator there is none. The feedwater line break characteristics dominate the steam line break characteristics. The steam line break cooldown towards the top of the generator is also very small. The inventory for the increased steam flow is depleted in ~ 1 second and the response of the generator then becomes one where an essentially adiabatic boundary condition exists on the water side of the tube and thermal fronts travel down the generator on

the sodium side unperturbed except by equilibration with the metal heat capacity. Figure 10 shows that in ~ 15 seconds after the blowdown the entire generator is at the sodium inlet nozzle temperature which for a first approximation is assumed to be constant.

Figures 11-13 show the temperatures in the metal at the slab node next to the sodium for the same three axial locations; sodium inlet nozzle, a midplane location and the sodium outlet nozzle. Figures 14-16 are the corresponding temperatures for the metal nodes next to the water side. The thermal stress problems are mitigated significantly by the short thermal time constant of the tubes ~ 0.5 seconds. It is the thicker structures such as nozzles which are more susceptible to thermal stress limitations. The implications of these results as the temperature fronts propagate through the remainder of the intermediate circuit await evaluation by structural stress codes.

ACKNOWLEDGEMENTS

This work was performed under the auspices of the U. S. Department of Energy.

REFERENCES

1. Y. I. Chang, J. F. Marchaterre, R. H. Sevy, "The Integral Fast Reactor Concept," Trans. Am. Nucl. Soc., 47, 293 (1984).

2. R. M. Singer et al., "Decay Heat Removal and Dynamic Plant Testing at EBR-II," Presented at 2nd Specialist's Meeting on Decay Heat Removal and Natural Convection in LMFBRs, Brookhaven National Laboratory, April 17-19, 1985.

3. J. P. Burelbach et al., "A New Approach to the Design of Core Support Structures for Large LMFBR Plants," pp. 1, Volume 2, Proceedings of the Conference on Structural Engineering in Nuclear Facilities, Raleigh, North Carolina, Sept. 10-12, 1984.

4. J. H. McFadden et al., "RETRAN-02 - A Program for Transient Thermal-Hydraulic Analysis of Complex Fluid Flow Systems. Volume 1: Equations and Numerics," Electric Power Research Institute Report, EPRI NP-1850-CCM, Vol. 1 (May 1981).

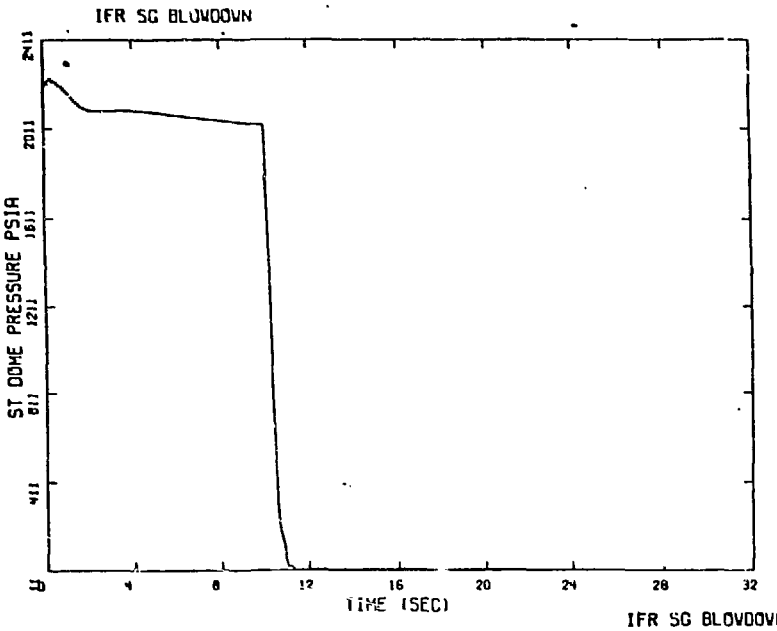

Figure 5. Steam Generator Pressure

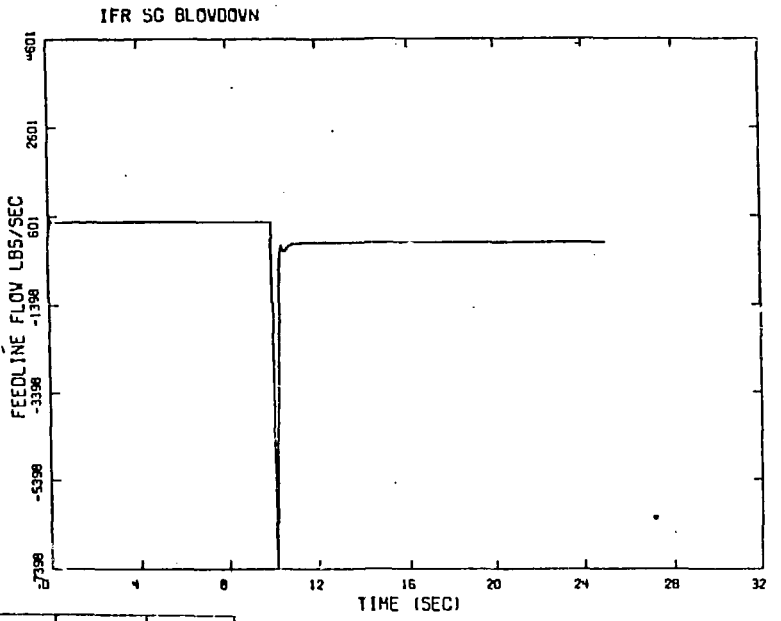

Figure 6. Feedwater Line Flow

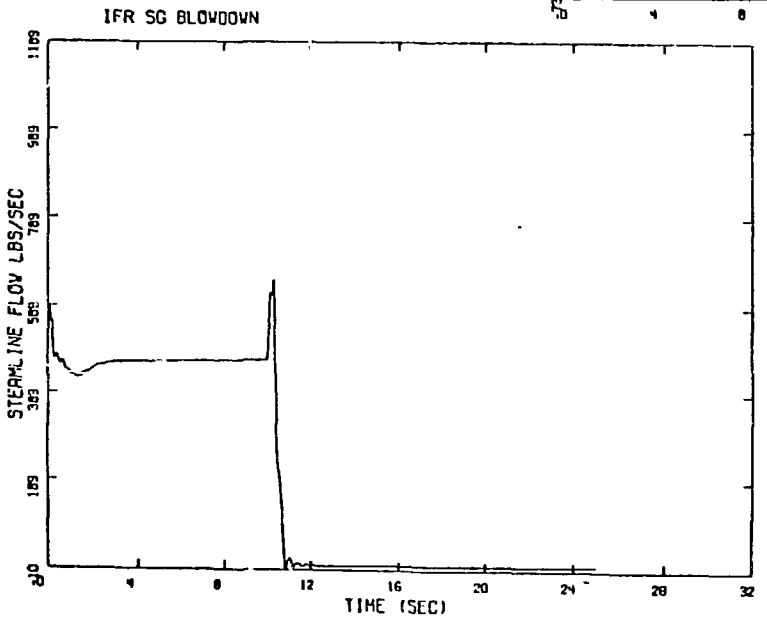

Figure 7. Steamline Flow

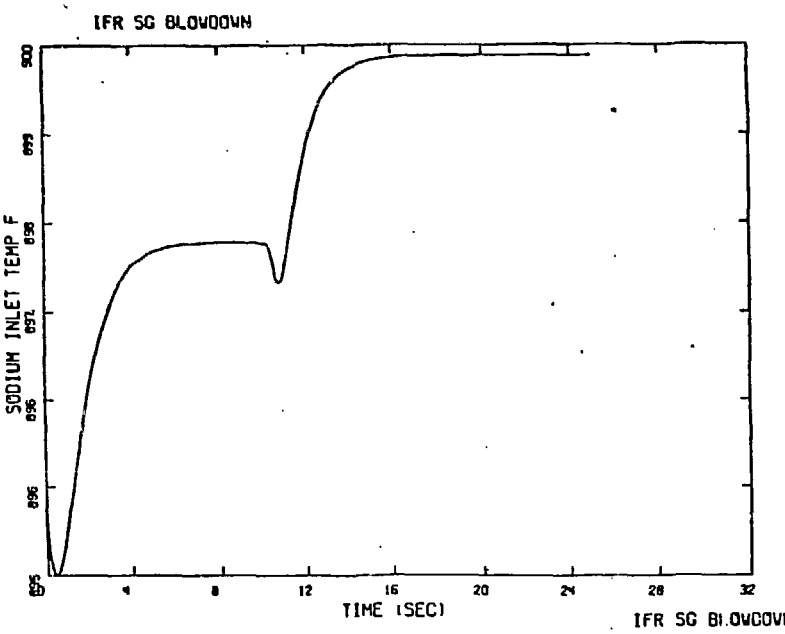

Figure 8. Sodium Temperature Inlet Nozzle

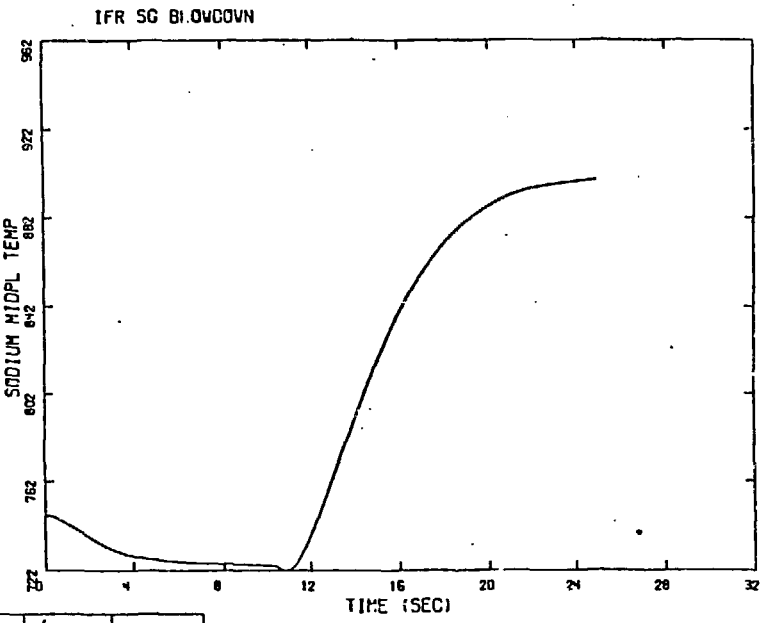

Figure 9. Sodium Temperature Midplane

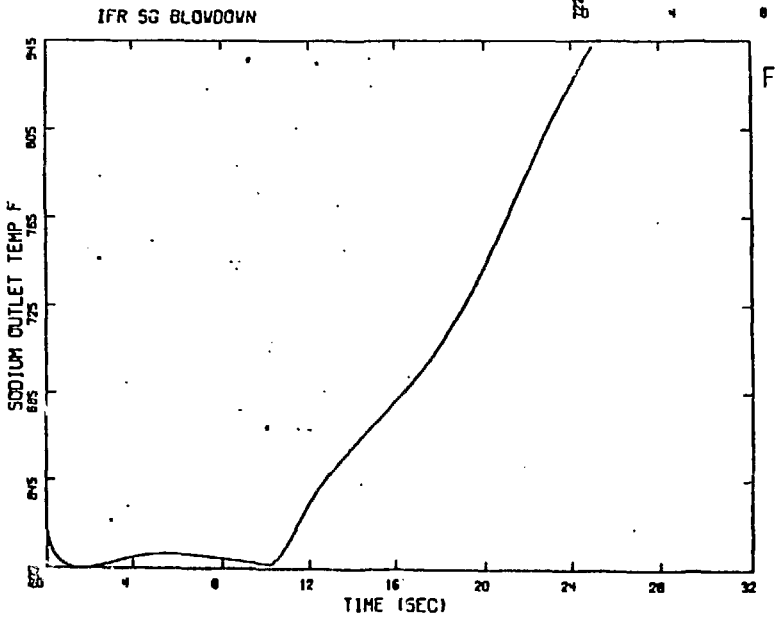

Figure 10. Sodium Temperature Outlet Nozzle

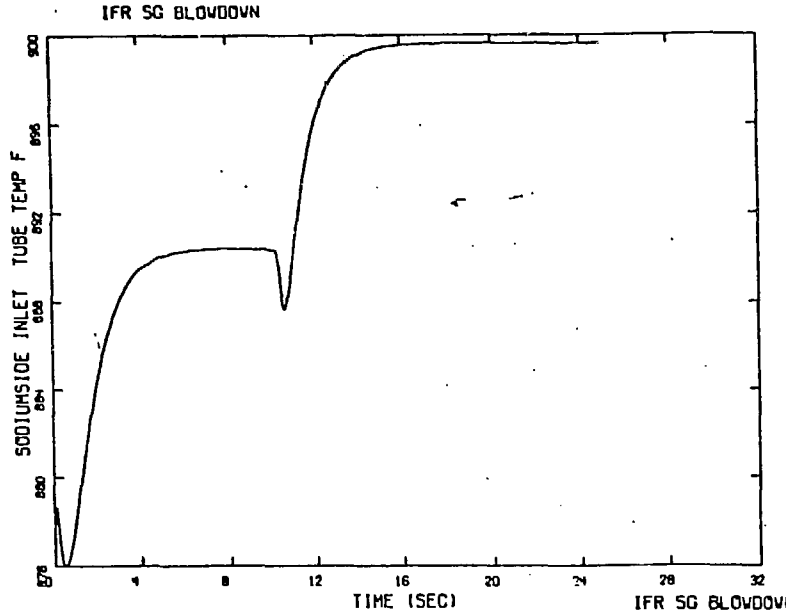

Figure 11. Sodium Side Tube Temperature Inlet Nozzle

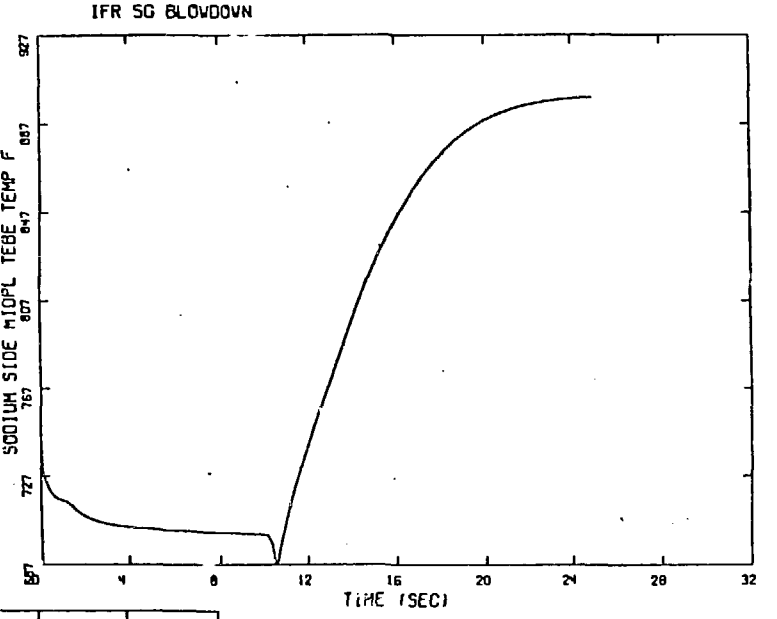

Figure 12. Sodium Side Tube Temperature Midplane

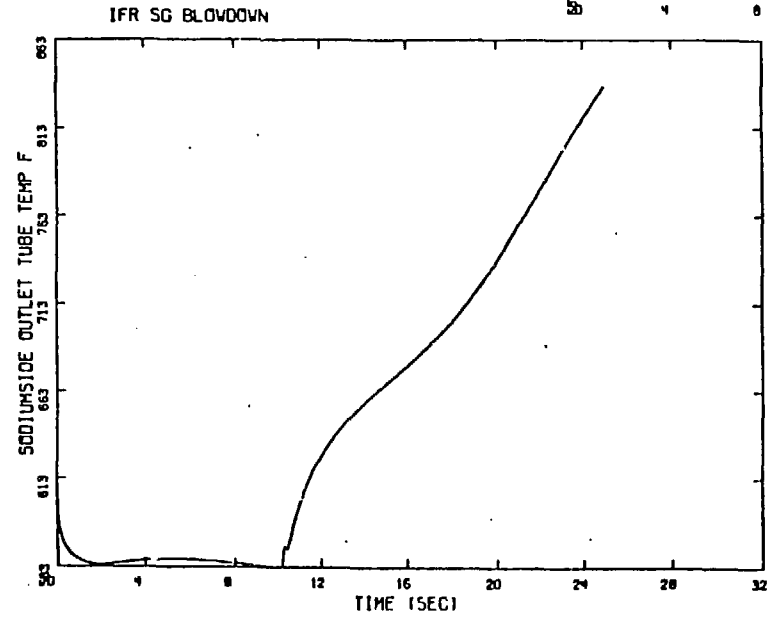

Figure 13. Sodium Side Tube Temperature Outlet Nozzle

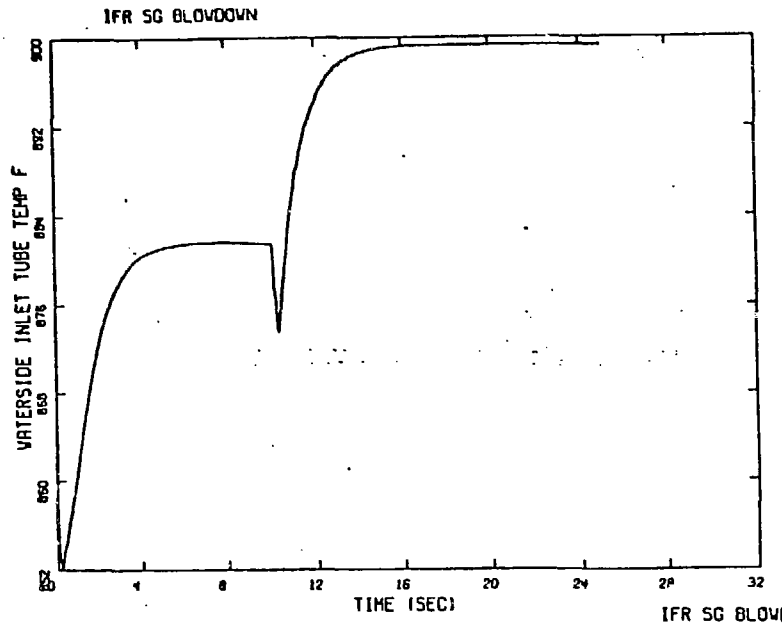

Figure 14. Water Side Tube Temperature Inlet Nozzle

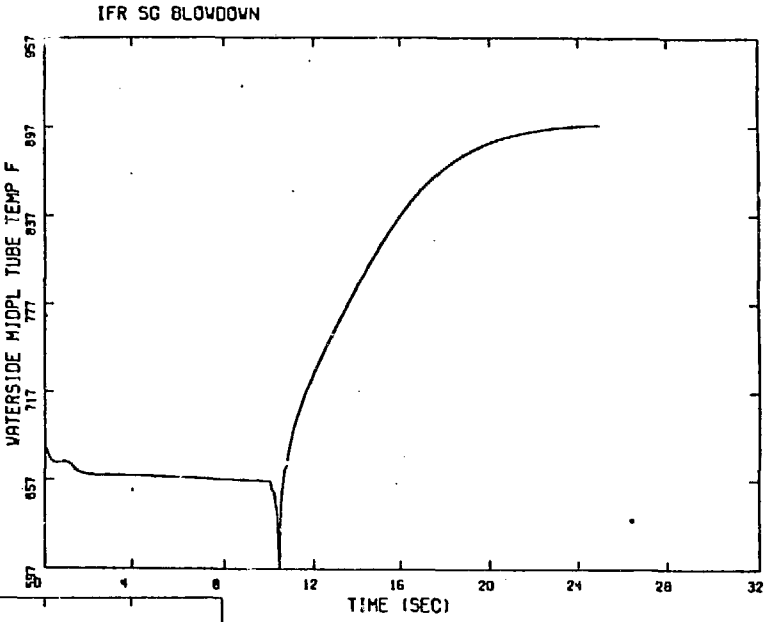

Figure 15. Water Side Tube Temperature Midplane

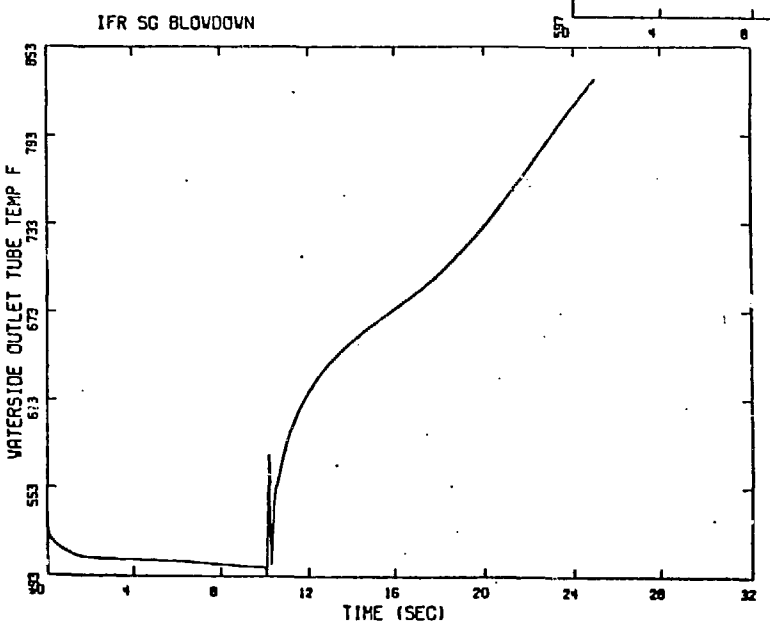

Figure 16. Water Side Tube Temperature Outlet Nozzle